


Explosive nucleosynthesis with fast neutrino-flavor conversion in core-collapse supernovae

Shin-ichiro Fujimoto¹ , Hiroki Nagakura²

¹*National Institute of Technology, Kumamoto College, Kumamoto 861-1102, Japan*

²*Division of Science, National Astronomical Observatory of Japan, 2-21-1 Osawa, Mitaka, Tokyo 181-8588, Japan*

Accepted XXX. Received YYY; in original form ZZZ

ABSTRACT

Fast neutrino (ν)-flavor conversion (FFC) is a possible game-changing ingredient in core-collapse supernova (CCSN) theory. In this *Letter*, we examine the impact of FFC on explosive nucleosynthesis by including the effects of FFC in conjunction with asymmetric ν emission into nucleosynthetic computations in a parametric way. We find that the ejecta compositions are not appreciably affected by FFC for elements lighter than Co while the compositions are influenced by FFC for the heavier elements. We also find that the role of FFC varies depending on the asymmetric degree of ν emission (m_{asy}) and the degree of ν -flavor mixing. The impact of FFC is not monotonic to m_{asy} ; The change in the ejecta composition increases for higher m_{asy} up to $\sim 10\%$ compared with that without FFC, whereas FFC has little effect on the nucleosynthesis in very large asymmetric ν emission ($\gtrsim 30\%$). Our results suggest that FFC facilitates the production of neutron-rich ejecta in most cases, although it makes the ejecta more proton-rich if anti- ν conversion is more vigorous than that of ν . The key ingredient accounting for this trend is ν absorption, whose effects on nucleosynthesis can be quantified by simple diagnostics.

Key words: stars: supernova: general – nuclear reactions, nucleosynthesis, abundances – neutrinos

1 INTRODUCTION

Core-collapse supernova (CCSN) explosion of a massive star chiefly produces elements heavier than oxygen through explosive nucleosynthesis, and expel them from the deep inside of the star (see, e.g., Sukhbold et al. 2016; Limongi & Chieffi 2018, and references therein). One of the ultimate goals of CCSN theory is to quantify how heavy elements can be synthesized, how large amounts of these elements are ejected from the star, and whether the abundance evolution observed on the surface of Galactic stars is well reproduced with a Galactic chemical evolution model with the contribution of CCSNe supplementing with those of other astrophysical sites, such as AGB stars and Type Ia SNe (see, e.g., Prantzos et al. (2018); Kobayashi et al. (2020)). Addressing these issues requires accurate modeling of neutrino (ν)-radiation-hydrodynamics since the nucleosynthetic yields sensitively depend on not only fluid dynamics but also the ν -radiation field. However, even the most recent CCSN models suffer from a big uncertainty of collective ν oscillations, posing a challenge to traditional nucleosynthesis

models. Offering key insights into the impact of collective ν oscillations is the subject of this *Letter*.

Detailed theoretical studies of collective ν oscillations indicate that the slow ν -flavor conversion, one of the collective oscillation modes, would be suppressed deep inside a CCSN core (Esteban-Pretel et al. 2008; Chakraborty et al. 2011; Sarikas et al. 2012). On the other hand, fast ν -flavor conversion (FFC) potentially overwhelms the matter suppression (see Tamborra & Shalgar 2020; Richers & Sen 2022; Capozzi & Saviano 2022, for recent reviews). In more recent years, detailed inspections of occurrences of FFCs have been made based on sophisticated multi-dimensional(D) CCSN models, and they commonly showed that electron neutrinos lepton number (ELN) crossing, which is a necessary and sufficient condition for the occurrence of FFC, appears ubiquitously in the accretion phase of CCSNe ($\lesssim 1$ s after the core bounce) (see, e.g., Abbar et al. 2021; Nagakura et al. 2021a; Harada & Nagakura 2022) spurring the interest of FFCs. These studies also exhibited that multi-D effects such as asymmetric ν emission offer favorable circumstances for the occurrence of FFC, although it is not clear how much they alter the explosive nucleosynthesis. The only reference in the literature is Xiong et al. (2020).

* E-mail: fuji@kumamoto-nct.ac.jp

The authors conducted nucleosynthetic computations in ν -driven winds at several hundred ms after the bounce, incorporating effects of FFCs based on spherically symmetric steady-state wind models.

In this *Letter*, we examine the impact of FFC induced by asymmetric ν emission on the explosive nucleosynthesis in multi-D CCSN models. By employing axisymmetric CCSN models in [Fujimoto & Nagakura \(2019, 2021\)](#), we carry out nucleosynthetic computation by incorporating FFC effects. The region of FFC is determined by a physically motivated criterion associated with the difference of ν emission among their species. We adopt a simple, phenomenological flavor-mixing scheme, although the scheme discards non-linear feedback from ν -radiation-hydrodynamics. This study possibly illustrates the essential features of the impact of FFC on nucleosynthesis, and will serve as a reference for higher-fidelity CCSN simulations with quantum kinetic ν transport.

This *Letter* is organized as follows. In section 2, we briefly summarize the method and results of axisymmetric CCSN simulations in our previous works ([Fujimoto & Nagakura 2019, 2021](#)). In section 3, we present our prescription by which to include the effects of FFC on nucleosynthetic computations. All results are encapsulated in section 4 with in-depth analyses of rolls of FFC on explosive nucleosynthesis. Finally, we summarize our conclusion in section 5.

2 HYDRODYNAMIC MODELS

In this study, we do not address all issues relevant to FFCs. Rather we focus on the roles of FFC on nucleosynthesis in CCSN. To this end, we adopt our CCSN hydrodynamic models ([Fujimoto & Nagakura 2019](#)), in which the effects of FFCs are neglected. We start with briefly summarizing the essence of our CCSN models.

We performed hydrodynamic simulations of CCSN from core collapse to runaway shock expansion for the $19.4M_{\odot}$ progenitor ([Woosley et al. 2002](#)). We employed two codes: GR1D ([O'Connor 2015](#)) in collapsing phase (spherically symmetric simulations) and a modified Zeus 2D code ([Stone & Norman 1992; Fujimoto et al. 2011](#)) for axisymmetric simulations in the post-bounce phase. Approximate ν transport is adopted for the modified Zeus 2D code with light-bulb prescription.

In our light-bulb ν -transport, the ν average energies are assumed to be spherically symmetric, which is a reasonable approximation indicated by more elaborate CCSN simulations ([Nagakura et al. 2019](#)). On the other hand, ν_e and $\bar{\nu}_e$ luminosities, L_{ν_e} and $L_{\bar{\nu}_e}$, respectively, can have large dipole components, meanwhile the ν_x and $\bar{\nu}_x$ luminosities, L_{ν_x} and $L_{\bar{\nu}_x}$, respectively, are assumed to be spherically symmetric. In our approach, the degree of dipole component is controlled by m_{asy} as,

$$L_{\nu_e} = L_{\nu_e, \text{ave}}(1 + m_{\text{asy}} \cos \theta), \quad (1)$$

$$L_{\bar{\nu}_e} = L_{\bar{\nu}_e, \text{ave}}(1 - m_{\text{asy}} \cos \theta), \quad (2)$$

where $L_{\nu_e, \text{ave}}$ and $L_{\bar{\nu}_e, \text{ave}}$ denote angular-averaged luminosities. For the sake of simplicity, the ratios of ν luminosities and average energies are assumed to be constant among models; $L_{\bar{\nu}_e, \text{ave}}/L_{\nu_e, \text{ave}} = 1$, $L_{\nu_x}/L_{\nu_e, \text{ave}} = L_{\bar{\nu}_x}/L_{\nu_e, \text{ave}} = 1/2$, and $\epsilon_{\bar{\nu}_e}/\epsilon_{\nu_e} = \epsilon_{\nu_x}/\epsilon_{\nu_e} = \epsilon_{\bar{\nu}_x}/\epsilon_{\nu_e} = 7/6$. and ϵ_{ν_e} , $\epsilon_{\bar{\nu}_e}$,

ϵ_{ν_x} , and $\epsilon_{\bar{\nu}_x}$ and the average energy of ν_e , $\bar{\nu}_e$, ν_x , and $\bar{\nu}_x$. To include the time-dependent features of ν luminosity and average energy, we use a ν -core model, which is essentially the same prescriptions in [Ugliano et al. \(2012\)](#). We ran the simulations for m_{asy} as 0%, 10/3%, 10%, 30%, and 50%¹. It is worth noting that m_{asy} is a pivotal factor to determine the spatial region where FFC occurs, as described in the next section.

3 PRESCRIPTION TO INCLUDE EFFECTS OF FFC IN NUCLEOSYNTHETIC COMPUTATIONS

According to recent studies of ELN crossings in CCSN (see, e.g., [Nagakura et al. 2021a](#)), the crossing appears around a ν sphere when the ratio of number density or flux between ν_e and $\bar{\nu}_e$ roughly equal each other. Our FFC instability criterion is built based on this trend and is given by

$$0.9 \leq \alpha_f \leq 1.1, \quad (3)$$

where $\alpha_f \equiv F_{\bar{\nu}_e}/F_{\nu_e}$. F_{ν_e} and $F_{\bar{\nu}_e}$ denote the number flux of ν_e and $\bar{\nu}_e$, respectively. By using Eqs. 1 and 2, we can express α_f as

$$\alpha_f = \frac{(L_{\bar{\nu}_e, \text{ave}}/\epsilon_{\bar{\nu}_e})}{(L_{\nu_e, \text{ave}}/\epsilon_{\nu_e})} \frac{1 - m_{\text{asy}} \cos \theta}{1 + m_{\text{asy}} \cos \theta} = \frac{6}{7} \frac{1 - m_{\text{asy}} \cos \theta}{1 + m_{\text{asy}} \cos \theta}, \quad (4)$$

since we set $L_{\bar{\nu}_e, \text{ave}} = L_{\nu_e, \text{ave}}$ and $\epsilon_{\nu_e}/\epsilon_{\bar{\nu}_e} = 6/7$ in our ν -core model.

Figure 1 portrays the corresponding region where FFC arises. In the case with $m_{\text{asy}} = 0\%$, no FFCs occur in the entire spatial region, because α_f is $6/7 (< 0.9)$. In other cases with asymmetric ν emission, FFC appears in the southern hemisphere, since ν_e ($\bar{\nu}_e$) emission is weaker (stronger) than that in the northern hemisphere. As a result, α_f can be higher than $6/7$ and satisfy the instability criterion (> 0.9) at a certain angular region. It should be mentioned, however, that α_f becomes higher than 1.1 around the southern pole for cases with $m_{\text{asy}} = 30\%$ and 50% ; consequently, FFCs are suppressed in these regions.

At present, global FFC simulations are unfeasible (but see [Nagakura & Zaizen 2022](#)) and no reliable approximations to include the effects of FFC have been established yet. We, hence, treat the degree of flavor-mixing in a parametric way, which is essentially the same as those used in [Xiong et al. \(2020\)](#); [Li & Siegel \(2021\)](#); [Just et al. \(2022\)](#); [Fernández et al. \(2022\)](#), but we alter the FFC criterion to suit CCSNe. One of the characteristics of FFC is that the flavor conversion is energy-independent². We, thus, introduce energy-independent parameters, p and \bar{p} , which exhibit the survival probabilities of ν_e and $\bar{\nu}_e$, respectively. The ν luminosity after the flavor conversion (L^{osc}) can be expressed by

¹ Recent ν -radiation-hydrodynamic simulations suggest that asymmetries of ν emission is $\lesssim 10\%$ (see, e.g., [Nagakura et al. 2021b](#), and references therein).

² However, ν -matter interactions may alter the trend; (see [Kato & Nagakura 2022](#), for more details).

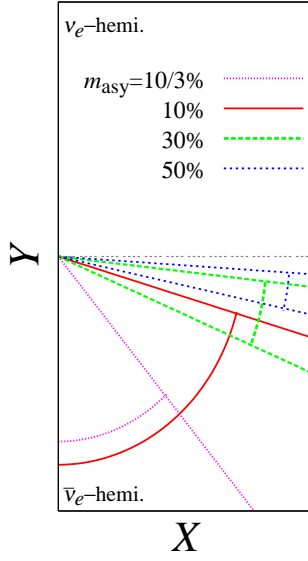


Figure 1. Spatial regions or angles where the FFC instability criterion (Eq. 3) is satisfied.

using the parameters,

$$L_{\nu_e}^{\text{osc}} = pL_{\nu_e} + (1-p)L_{\nu_x}, \quad (5)$$

$$L_{\bar{\nu}_e}^{\text{osc}} = \bar{p}L_{\bar{\nu}_e} + (1-\bar{p})L_{\bar{\nu}_x}, \quad (6)$$

$$L_{\nu_x}^{\text{osc}} = \frac{1}{2}(1-p)L_{\nu_e} + \frac{1}{2}(1+p)L_{\nu_x}, \quad (7)$$

$$L_{\bar{\nu}_x}^{\text{osc}} = \frac{1}{2}(1-\bar{p})L_{\bar{\nu}_e} + \frac{1}{2}(1+\bar{p})L_{\bar{\nu}_x}. \quad (8)$$

In this study, we adopt five sets of (p, \bar{p}) ; three symmetric FFC cases, or $(p, \bar{p}) = (1, 1)$ (no FFC), $(2/3, 2/3)$, and $(1/3, 1/3)$ (flavor equilibrium) and two asymmetric FFC cases, $(2/3, 1/3)$ and $(1/3, 2/3)$. We then carry out the nucleosynthetic computations by the same method as described in our previous papers (Fujimoto & Nagakura 2019, 2021), but we use L^{osc} in the ν -matter interactions.

4 RESULTS

We present mass distribution in electron fraction, Y_e , which is useful to catch the overall trend of the impact of FFC on nucleosynthesis. The ejecta mass in a bin of $dY_{e,1} = 0.005$, dM_{ej} , is displayed in Figure 2, where $Y_{e,1}$ denotes the electron fraction when the temperature of each fluid element becomes 10^9 K, approximately reflecting the freeze-out value of Y_e . The dependence of dM_{ej} on p and \bar{p} exhibits the effects of FFCs, and it also varies with m_{asy} . To see the m_{asy} dependence, we compare the two cases with $m_{\text{asy}} = 10\%$ (top) and 30% (bottom) in Figure 2. As shown in the bottom panels, dM_{ej} distribution is less sensitive to p and \bar{p} in the case with $m_{\text{asy}} = 30\%$, indicating that effects of FFCs are minor. This is due to the fact that FFCs are suppressed around the pole in the southern hemisphere (see Fig. 1) due to a substantial excess of $\bar{\nu}_e$ compared to ν_e . A similar trend is also found in the case with $m_{\text{asy}} = 50\%$.

In the case of $m_{\text{asy}} = 10\%$, the dependence of dM_{ej} distributions on p and \bar{p} is more remarkable than $m_{\text{asy}} = 30\%$ (see the top panels in Fig. 2). In the symmetric FFC case ($p = \bar{p}$), FFC does not affect dM_{ej} distribution at $Y_{e,1} \gtrsim 0.5$

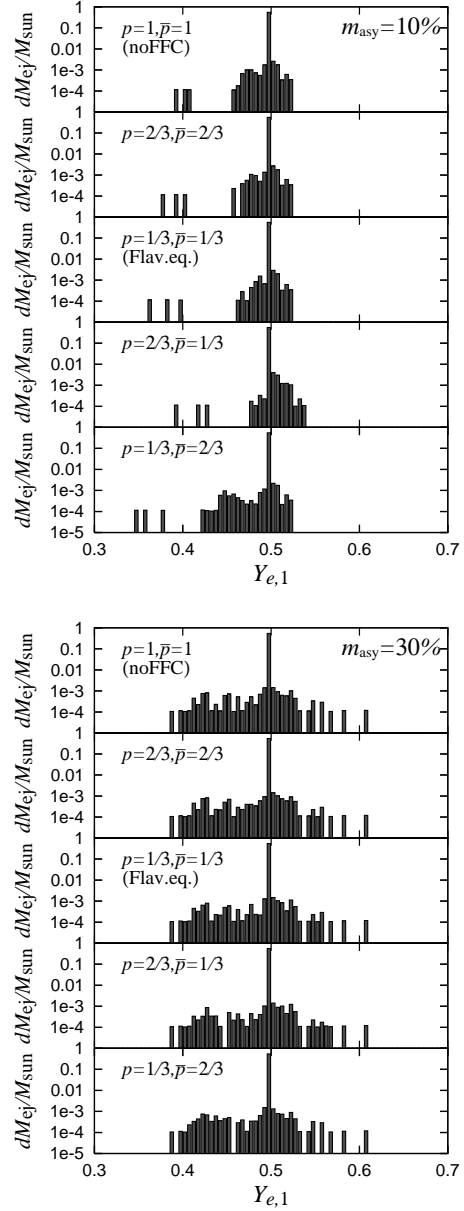


Figure 2. dM_{ej} as a function of freeze-out electron fraction, $Y_{e,1}$. We focus on the ejecta that is located at $\leq 10,000$ km at the onset of gravitational collapse. We show results for $m_{\text{asy}} = 10\%$ (top) and 30% (bottom). In each figure, we display the results with $(p, \bar{p}) = (1, 1)$ (no FFC), $(2/3, 2/3)$, and $(1/3, 1/3)$ (flavor equilibrium), $(2/3, 1/3)$ and $(1/3, 2/3)$ from top to bottom.

(see the top three panels). This is attributed to the fact that the proton-rich ejecta appears in the ν_e -rich hemisphere, where no FFC arises. In the neutron-rich side ($Y_{e,1} \lesssim 0.5$), dM_{ej} distribution tends to shift to lower $Y_{e,1}$ with decreasing $p(=\bar{p})$. In asymmetric FFC cases ($p \neq \bar{p}$), it substantially deviates from the case with no FFCs. The ejecta becomes more neutron-rich for $(p, \bar{p}) = (1/3, 2/3)$, while more proton-rich for $(p, \bar{p}) = (2/3, 1/3)$. These trends can be understood through the balance of ν_e and $\bar{\nu}_e$ absorptions, as we shall discuss the detail with Figure 5. It should also be mentioned that the same trend is observed in the case of $m_{\text{asy}} = 10/3\%$, albeit less significantly than $m_{\text{asy}} = 10\%$. This is due to narrower spatial region where FFC occurs (see Fig. 1).

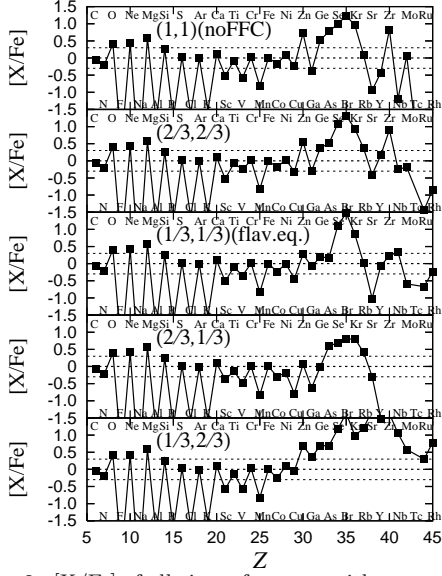


Figure 3. $[X/Fe]$ of all ejecta for cases with $m_{\text{asy}} = 10\%$ and with $(p, \bar{p}) = (1, 1)$ (no FFC), $(2/3, 2/3)$, and $(1/3, 1/3)$ (flavor equilibrium), $(2/3, 1/3)$ and $(1/3, 2/3)$ in panels from top to bottom.

Hereafter we focus on the case with $m_{\text{asy}} = 10\%$, in which FFC gives the largest impact on nucleosynthesis among our models. In Figure 3, the ejecta compositions are displayed as a function of atomic number Z , and the abundance pattern is measured with $[X/Fe]$ ³. We find that FFC facilitates the production of heavier elements ($Z \geq 28$), unless $\bar{\nu}$ flavor conversion is remarkably higher than that of ν (corresponding to $(p, \bar{p}) = (2/3, 1/3)$ in our model). This trend is consistent with dM_{ej} distributions in $Y_{e,1}$, i.e., increasing the mass of neutron-rich matter, as displayed in Figure 2. On the other hand, elements lighter than Co ($Z \leq 27$) other than Sc and V, which are abundantly produced in slightly proton- and neutron-rich ejecta, respectively, are less sensitive to FFCs. This is attributed to the fact that the mass of the ejecta with $Y_{e,1} \simeq 0.5$, in which the elements lighter than Co are chiefly produced, is less influenced by ν absorption and thus by FFCs.

To understand the mechanism of how FFC gives impact on FFC, we show the trajectory and the time evolution of Y_e for neutron-rich ejecta by focusing on three individual particles having the lowest $Y_{e,1}$. In the following discussions, we refer to these particles as P1, P2, and P3 in order of increasing $Y_{e,1}$ (0.390, 0.400, and 0.409 for P1, P2, and P3 in the case without FFC, respectively). Figure 4 depicts the trajectories of these particles. We note that the trajectories are independent of p and \bar{p} for each particle since the fluid background is identical among models with a different set of p and \bar{p} . As shown in the figure, all particles reach near the ν sphere, suggesting that they experience strong depletion. We also find that they pass through the region around the southern pole, indicating that they are influenced by FFC (see also Fig. 1).

The rolls of FFCs on ejecta compositions can be inter-

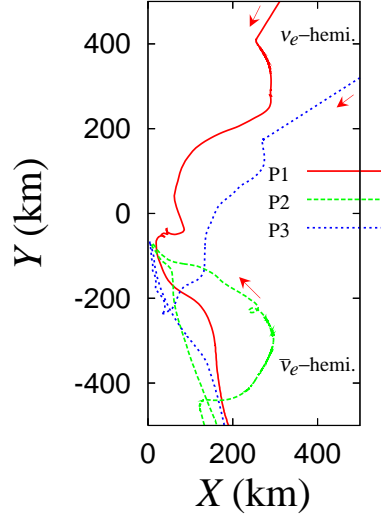


Figure 4. Trajectories of three tracer particles with the lowest $Y_{e,1}$. All particles eject through the $\bar{\nu}_e$ -hemisphere, where the FFC appears.

preted through the time evolution of Y_e for these individual particles, which are displayed in Figure 5. As a reference, we also show the radial position of each particle as a blue line. Before entering into a detailed discussion of FFC, we briefly describe the essential time-dependent features of Y_e in the case without FFC (see red line in the figure). After passing through the accretion shock wave, Y_e of each particle rapidly decreases mainly due to electron capture on protons. Once the shock revival is achieved, the ejecta experiences expansion, and then ν absorption dictates the evolution of Y_e . In general, ν_e absorption on neutrons dominates over $\bar{\nu}_e$ one on protons, indicating that Y_e increases with time. It should be noted, however, that the increase of Y_e is suppressed in the region with high $\bar{\nu}_e$ emission (southern hemisphere in our models), which leads to lower $Y_{e,1}$.

Let us now turn our attention to the cases with FFCs. As displayed in Figure 5, the time evolution of Y_e clearly depends on the choice of (p, \bar{p}) . The key effect of FFC is the reduction of ν absorption, which can be understood through the following analysis. We start with defining the absorption factor with FFC as, $f_{\nu_e, \text{osc}} \equiv \epsilon_{\nu_e}^2 p F_{\nu_e} + \epsilon_{\nu_x}^2 (1-p) F_{\nu_x}$, which is roughly proportional to the ν_e absorption rate. We then take the ratio to the case without FFC (i.e., $f_{\nu_e} = \epsilon_{\nu_e}^2 F_{\nu_e}$) as,

$$\begin{aligned} \frac{f_{\nu_e, \text{osc}}}{f_{\nu_e}} &= p(1 + m_{\text{asy}} \cos \theta) + \frac{L_{\nu_x}}{L_{\nu_e, \text{ave}}} \frac{\epsilon_{\nu_x}}{\epsilon_{\nu_e}} (1-p) \\ &= \frac{5p+7}{12} + p m_{\text{asy}} \cos \theta. \end{aligned} \quad (9)$$

The first term on the right-hand side of Eq. 9 is much larger than the second one unless m_{asy} is an order of unity. This indicates that the ratio of absorption factor to that without FFC monotonically decreases with p , exhibiting that the ν_e absorption becomes weaker when p is smaller, or the ν -flavor conversion becomes more active. The same argument can be applied to $\bar{\nu}_e$. We obtain the following relation,

$$\frac{f_{\bar{\nu}_e, \text{osc}}}{f_{\bar{\nu}_e}} = \frac{\bar{p}+1}{2} - \bar{p} m_{\text{asy}} \cos \theta, \quad (10)$$

³ $[A/B] \equiv \log [(X_A/X_{A,\odot})/(X_B/X_{B,\odot})]$, where X_i and $X_{i,\odot}$ denote a mass fraction of element i and its solar value (Anders & Grevesse 1989).

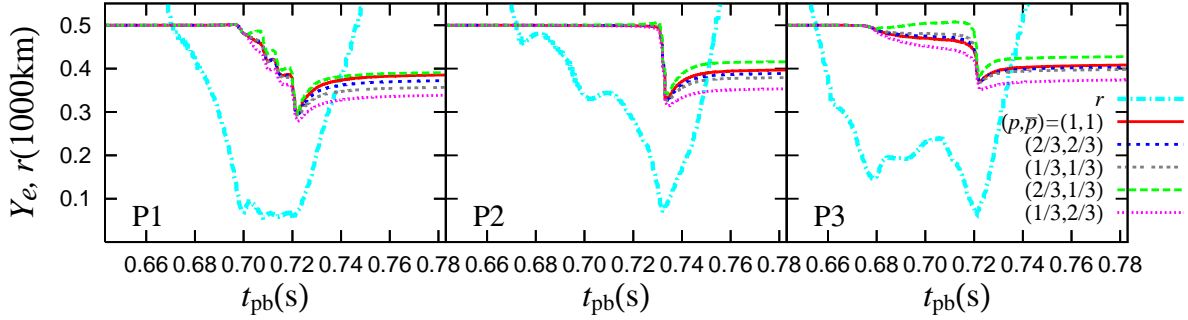


Figure 5. Time evolution of Y_e and radial position, r , of the three ejecta with the lowest $Y_{e,1}$, whose trajectories are shown in Fig. 4, for cases with $m_{\text{asy}} = 10\%$ and with $(p, \bar{p}) = (1, 1)$ (no FFC), $(2/3, 2/3)$, $(1/3, 1/3)$ (flavor equilibrium), $(2/3, 1/3)$ and $(1/3, 2/3)$.

suggesting that $\bar{\nu}_e$ absorption becomes also less efficient for stronger $\bar{\nu}_e$ -flavor conversion.

The reduction of ν absorption leads to two important effects on the evolution of Y_e , which depends on p and \bar{p} . First, the increase of Y_e is suppressed during the ejecta expansion; the trend can be seen in the symmetric FFC (see blue and gray lines in Figure 5). This accounts for the increased mass of neutron-rich ejecta. Second, the ratio between ν_e and $\bar{\nu}_e$ absorptions can be substantially altered in the asymmetric FFCs ($p \neq \bar{p}$). More specifically, Y_e tends to be lower in the case of $p < \bar{p}$ (see pink lines in Fig. 5), since ν_e absorption is more suppressed than $\bar{\nu}_e$ one. In the opposite case $p > \bar{p}$ (see green lines in the same figure), FFC makes the ejecta more proton-rich; in fact the maximum $Y_{e,1}$ in the case with $(p, \bar{p}) = (2/3, 1/3)$ becomes remarkably higher than that without FFC (see Fig. 2).

A few remarks should be made now. The roles of FFC on nucleosynthesis is qualitatively changed if $L_{\nu_x} \epsilon_{\nu_x}$ and $L_{\bar{\nu}_x} \epsilon_{\bar{\nu}_x}$ are larger than those of ν_e and $\bar{\nu}_e$, respectively. In these cases, FFC boosts the efficiency of ν absorption. On the other hand, recent CCSN simulations suggest that $L_{\nu_x} \epsilon_{\nu_x}$ and $L_{\bar{\nu}_x} \epsilon_{\bar{\nu}_x}$ do not overwhelm those of ν_e and $\bar{\nu}_e$ during the accretion phase (see, e.g., Nagakura et al. 2021b), suggesting that the present results captures the essential roles of FFC on explosive nucleosynthesis relevant to recent CCSN models. Next, Xiong et al. (2020) has shown that ν -driven winds become more proton-rich if the effects of FFC are included. Their results are consistent with ours, since they adopt $p = 0.68$ and $\bar{p} = 0.55$ in their simulations, suggesting that $\bar{\nu}_e$ absorption is more suppressed than ν_e one by FFCs. As such, Eqs. 9 and 10 are very useful to gaze into the sensitivity of nucleosynthesis on FFC for arbitrary systems. It should be mentioned, however, that our models neglect the feedback effects of FFC through ν -radiation-hydrodynamics. This suggests that more complex effects of FFC on nucleosynthesis may arise in reality. In fact, the complex interplay between fluid-dynamics, nucleosynthesis, and FFC has been already observed in NS merger systems (Li & Siegel 2021; Just et al. 2022; Fernández et al. 2022). We postpone addressing this important issue in future work.

5 CONCLUSION

CCSNe involving asymmetric ν emission potentially have FFC around a ν sphere. In this Letter, we examine the impact of FFC on the explosive nucleosynthesis in such aspherical CCSNe under the assumption that FFC does not affect fluid dynamics. The main results are summarized as follows.

(i) FFC appears in the $\bar{\nu}_e$ -enhanced region, in which the $\bar{\nu}_e$ luminosity is larger than the ν_e one. The impact of FFC on nucleosynthesis increases with m_{asy} but it is suppressed for large ν asymmetry ($m_{\text{asy}} \gtrsim 30\%$) due to the narrower spatial region where FFC appears.

(ii) FFC has little effect on abundances of elements lighter than Co other than Sc and V since the elements are mainly produced in the region where ν -absorption is weak.

(iii) For the symmetric FFC cases ($p = \bar{p}$), FFC makes the ejecta more neutron-rich. Consequently, the ejecta has larger amounts of elements heavier than Ni (Figs. 2 and 3). For asymmetric FFC cases ($p \neq \bar{p}$), the ejecta become more neutron- and proton-rich for $p < \bar{p}$ and $p > \bar{p}$, respectively, compared to the case without FFC.

(iv) Those dependences of nucleosynthesis on the degree of flavor mixing (p and \bar{p}) can be understood through the ν_e and $\bar{\nu}_e$ absorption. Eqs. 9 and 10 provides a simple but essential diagnostics to quantify how FFC changes ν absorption.

6 ACKNOWLEDGEMENTS

This work is partly supported by JSPS KAKENHI Grant Number 20K03957.

DATA AVAILABILITY

The data underlying this article will be shared upon reasonable request to the corresponding author.

REFERENCES

- Abbar S., Capozzi F., Glas R., Janka H. T., Tamborra I., 2021, *Phys. Rev. D*, **103**, 063033
- Anders E., Grevesse N., 1989, *Geochimica Cosmochimica Acta*, **53**, 197
- Capozzi F., Saviano N., 2022, *Universe*, **8**, 94
- Chakraborty S., Fischer T., Mirizzi A., Saviano N., Tomàs R., 2011, *Phys. Rev. Lett.*, **107**, 151101
- Esteban-Pretel A., Mirizzi A., Pastor S., Tomàs R., Raffelt G. G., Serpico P. D., Sigl G., 2008, *Phys. Rev. D*, **78**, 085012
- Fernández R., Richers S., Mulyk N., Fahlman S., 2022, arXiv e-prints, p. arXiv:2207.10680
- Fujimoto S.-i., Nagakura H., 2019, *MNRAS*, **488**, L114
- Fujimoto S.-i., Nagakura H., 2021, *MNRAS*, **502**, 2319
- Fujimoto S.-i., Kotake K., Hashimoto M.-a., Ono M., Ohnishi N., 2011, *ApJ*, **738**, 61
- Harada A., Nagakura H., 2022, *ApJ*, **924**, 109
- Just O., Abbar S., Wu M.-R., Tamborra I., Janka H.-T., Capozzi F., 2022, *Phys. Rev. D*, **105**, 083024

- Kato C., Nagakura H., 2022, arXiv e-prints, p. [arXiv:2207.09496](#)
- Kobayashi C., Karakas A. I., Lugaro M., 2020, *ApJ*, **900**, 179
- Li X., Siegel D. M., 2021, *Phys. Rev. Lett.*, **126**, 251101
- Limongi M., Chieffi A., 2018, *The Astrophysical Journal Supplement Series*, **237**, 13
- Nagakura H., Zaizen M., 2022, arXiv e-prints, p. [arXiv:2206.04097](#)
- Nagakura H., Sumiyoshi K., Yamada S., 2019, *ApJ*, **880**, L28
- Nagakura H., Burrows A., Johns L., Fuller G. M., 2021a, *Phys. Rev. D*, **104**, 083025
- Nagakura H., Burrows A., Vartanyan D., Radice D., 2021b, *MNRAS*, **500**, 696
- O'Connor E., 2015, *ApJS*, **219**, 24
- Prantzos N., Abia C., Limongi M., Chieffi A., Cristallo S., 2018, *MNRAS*, **476**, 3432
- Richers S., Sen M., 2022, arXiv e-prints, p. [arXiv:2207.03561](#)
- Sarikas S., Tamborra I., Raffelt G., H  depohl L., Janka H.-T., 2012, *Phys. Rev. D*, **85**, 113007
- Stone J. M., Norman M. L., 1992, *ApJS*, **80**, 753
- Sukhbold T., Ertl T., Woosley S. E., Brown J. M., Janka H.-T., 2016, *ApJ*, **821**, 38
- Tamborra I., Shalgar S., 2020, arXiv e-prints, p. [arXiv:2011.01948](#)
- Ugliano M., Janka H.-T., Marek A., Arcones A., 2012, *ApJ*, **757**, 69
- Woosley S. E., Heger A., Weaver T. A., 2002, *Reviews of Modern Physics*, **74**, 1015
- Xiong Z., Sieverding A., Sen M., Qian Y.-Z., 2020, *ApJ*, **900**, 144

This paper has been typeset from a $\text{\TeX}/\text{\LaTeX}$ file prepared by the author.